Journal of Geodesy (2026) 100:89
https://doi.org/10.1007/s00190-026-02102-4

ORIGINAL ARTICLE

Sequential integral inversion in regional gravity field modelling

Mehdi Eshagh[1,2]

Received: 5 March 2026 / Accepted: 22 July 2026 / Published online: 1 October 2026
© The Author(s) 2026

Abstract

Two sequential strategies for the integral inversion of multi-platform gravimetric observations are presented for regional gravity field modelling. In contrast to conventional batch solutions, the proposed approaches enable the progressive combination of large, heterogeneous and ill-conditioned systems while preserving full stochastic information. In the first, a priori background information and its variance–covariance matrix (VCM) are incorporated in a formulation conceptually analogous to data assimilation, allowing the sequential update of the solution and its precision measures. In the second, multiple ill-conditioned systems derived from discretised integral equations are combined sequentially without external background information. For both approaches, rigorous models are derived for the sequential propagation and combination of observations, VCMs, a posteriori variances and regularisation-induced biases within a Tikhonov regularisation framework. The methods are applied to the gravity field and steady-state ocean circulation explorer (GOCE) gravity gradient data over Central Europe during August–September 2013. A total of 94,540 observations are divided into ten subsets and processed sequentially to recover gravity anomalies at sea level. The results are compared with a conventional batch inversion. When reliable background information is available, the first algorithm yields stable and consistent solutions. The second algorithm produces results largely equivalent to the batch solution, with differences generally below 1 mGal in standard deviation. The proposed formulation provides a computationally feasible and fully stochastic alternative to batch integral inversion for large gravimetric data sets and enables the consistent integration of multi-platform observations in regional gravity field modelling.

Keywords Data assimilation · Ill-conditioned systems · Sequential integral inversion · Tikhonov regularisation · Variance—covariance matrix

1 Introduction

The rapid growth in the volume and heterogeneity of modern gravimetric observations has fundamentally changed the numerical requirements of regional gravity field modelling. Satellite missions, airborne surveys, and dense terrestrial measurements now provide data sets whose size often renders classical batch least-squares inversion computationally demanding or even impractical. In integral approaches, discretisation of the governing relations leads to large and severely ill-conditioned systems of equations, for which the simultaneous estimation of the unknown parameters, their variance–covariance information, and the regularisation terms becomes increasingly difficult as the data volume grows. These challenges motivate the development of solution strategies that allow the information content of large data sets to be incorporated progressively rather than through a single global adjustment. The present study develops two sequential algorithms addressing this issue, with emphasis on the integral inversion of satellite gradiometry data.

Early integral formulations for recovering gravity anomalies from satellite gradients were established by Reed (1973), who derived relations based on second-order derivatives of the generalised Stokes integral. Because discretisation of these relations leads to ill-conditioned systems, stabilisation techniques became essential. Xu (1992, 1998) introduced Tikhonov regularisation (Tikhonov 1963; Tikhonov and Arsenin 1977) and truncated singular value decomposition for such problems, including strategies for estimating regularisation parameters. Subsequent developments addressed alternative formulations and stabilisation strategies, including local frame integral equations (Kern and Haagmans

✉ Mehdi Eshagh
mehdi.eshagh@smhi.se

[1] Division of Forecast and Observations, Department of Research and Development, Swedish Meteorological and Hydrological Institute (SMHI), Norrköping, Sweden

[2] Department of Applied Geomatics, University of Sherbrooke, Sherbrooke, Quebec, Canada

2005), geocentric formulations (Janák et al. 2009), covariance adaptive regularisation (Kotsakis 2007), and iterative schemes for the joint estimation of regularisation parameters and variance components (Xu 2009). Further studies focussed on mitigating spatial truncation error (STE) and improving inversion performance. Modifications of the integral formulae and recovering strategies were investigated to reduce truncation effects and improve accuracy (Eshagh 2011a, b). A sequential version of Tikhonov regularisation was later proposed (Eshagh 2011c), in which the regularisation parameter estimated from an initial data set is subsequently applied to additional observations and bias correction. Other approaches include near–far zone separation for GOCE gradients (Pitoňák et al. 2017), least-squares collocation (Saadat et al. 2019), spectral combination methods for downward continuation (Pitoňák et al. 2020, 2023), and radial basis function representations (Schmidt et al. 2006; Eicker 2008; Eicker et al. 2014; Naeimi and Bouman 2017). More recently, Eshagh et al. (2025) analysed several direct integral inversion schemes for the gravity field and steady-state ocean circulation explorer (GOCE, ESA 1999) data from the perspective of uncertainty propagation in batch processing.

In all of the aforementioned studies, increasing data volume substantially complicates the solution of the discretised integral equations. As system dimensionality grows, ill-conditioning becomes more pronounced, rendering direct regularisation computationally expensive and, for large data sets, sometimes impractical. This situation calls for alternative numerical strategies that ensure stable and efficient handling of large-scale problems. In contrast to previously published direct inversion approaches, the present study develops a stochastic sequential framework for the progressive combination of large gravimetric data sets. Whereas Eshagh et al. (2025) focussed on uncertainty propagation within batch integral inversion schemes, the emphasis here is on reformulating the estimation procedure itself to enable stable sequential processing of large ill-conditioned systems.

In contrast to classical sequential least-squares or Kalman filtering methods, which generally leads to solving well-conditioned systems, the present formulation is designed explicitly for the sequential solution of ill-conditioned systems, derived after discretisation of integral formulae. The proposed framework introduces three principal conceptual advances. First, Tikhonov regularisation is embedded directly into each sequential update, while the associated regularisation biases are consistently propagated throughout all inversion cycles. This enables stable and mathematically consistent sequential estimation in ill-conditioned settings, which need special attention to regularisation bias. Second, two algorithmic variants are developed. The first incorporates a background model together with its variance–covariance matrix (VCM), in which successive subsets of observations update the background state through correction vectors derived from the observation–model misfit, yielding progressively refined estimates. The second applies the sequential strategy directly to the discretised integral equations, where partial normal equations are accumulated and updated as new data blocks are introduced. Third, a complete mathematical framework is established for the propagation and updating of VCMs, together with the estimation of the variance of unit weight, for both algorithmic variants.

These developments extend the sequential regularisation method of Eshagh (2011c) into a comprehensive stochastic formulation for integral inversion. Whereas the earlier approach relied on a single regularisation parameter—whose quality strongly influenced all subsequent steps and whose uncertainty propagated through the entire sequence—the present work avoids this limitation by explicitly modelling the VCMs and the a posteriori variance of unit weight at each stage. The methods are demonstrated using GOCE data over Europe, and the sequential solutions are compared with conventional batch inversion. Although the formulation is expressed in spherical coordinates, which is natural for satellite gravimetry, this representation introduces geometric simplifications relative to the physical reality of the Earth's surface. However, this inversion framework is general and applicable to sequential solutions of integral equations in any coordinate system for a wide range of geodetic and geophysical problems.

2 Integral equation

Consider the integral equation relating the second-order radial derivative of the disturbing potential T_{rr} at the satellite orbit to the gravity anomaly (Δg) at mean sea level:

$$T_{rr}(r,\,\Omega) = \frac{R}{4\pi}\iint_{\Omega_0} S_{rr}(r,\,\psi,\,R)\Delta g\big(R,\,\Omega'\big)\mathrm{d}\Omega' \qquad (1a)$$

where R, r and ψ, respectively, stand for the radius of the mean geocentric sphere approximating mean sea level, the geocentric distance of the computation point $\Omega = (\phi,\,\lambda)$, where ϕ and λ are, respectively, latitude and longitude at the satellite orbit and ψ is the spherical geocentric angle between computation and the integration point $\Omega' = (\phi',\,\lambda')$, ($\phi'$ latitude and λ' longitude of the integration point). Ω_0 is the integration domain and $\mathrm{d}\Omega'$ the surface integration element on it. The kernel of the integral formula (1a) is (Reed 1973):

$$S_{rr}(r,\psi,R)=\frac{t^3}{R^2}\left[(1-tx)\left(\frac{3(1-t^2)}{D^5}-\frac{4}{D^3}\right)-\frac{1+t^2}{D^3}-\frac{10}{D}-18D+2 -3tx\left(15+6\ln\frac{1-tx+D}{2}\right)\right] \tag{1b}$$

where $t=r/R$, $D=\sqrt{1-2tx+t^2}$ and $x=\cos\psi$.

Discretisation of Eq. (1a) leads to an observation equation connecting a single T_{rr} to Δg at sea level in a gridded integration domain with a desired resolution. When the number of measured T_{rr} is larger than that of Δg; therefore, an overdetermined system of linear equations is obtained, which is normally solved for Δg by the least-squares method. Its solution must further be regularised as this system is ill-conditioned and sensitive to noise of T_{rr}. For estimating the VCM of the estimated Δg, different methods based on a posteriori variance factors or variance components have been developed; see e.g. Xu et al. (2006) and Eshagh et al. (2025). In the following section, we will present how the discretised form of the integral (1a) is combined with background data, or a priori values of the unknowns and their VCM.

3 Sequential integral inversion using background data

Here, an approach conceptually similar to data assimilation methods (e.g. Kalnay et al. 2024) is developed. Unlike classical data assimilation, however, one of the systems involves unknown parameters that are effectively observed through external sources, such as a global Earth Gravitational Model (EGM) or a local/regional gravity model. The second system of equations arises from the discretisation of an integral equation (e.g. Eq. 1a) and is typically ill-conditioned.

The first system, therefore, represents prior information in which the unknown parameters are directly observed or taken from independent models, whereas the second system provides indirect observational relation through integral relations. In the following, these two systems are formulated explicitly, and the procedure by which they are combined in a sequential manner is described. We begin with the first system:

$$\mathbf{x}_\mathrm{b}=\mathbf{x}+\boldsymbol{\varepsilon}_\mathrm{b}\ \text{with}\ \mathrm{E}\{\boldsymbol{\varepsilon}_\mathrm{b}\}=0\ \text{and}\ \mathrm{E}\left\{\boldsymbol{\varepsilon}_\mathrm{b}\boldsymbol{\varepsilon}_\mathrm{b}^\mathrm{T}\right\}=\sigma_\mathrm{b}^2\mathbf{B} \tag{2a}$$

where $\mathbf{x}_\mathrm{b}$ is called background vector, which is an estimate of $\mathbf{x}$, the vector of true values, $\boldsymbol{\varepsilon}_\mathrm{b}$ is the uncertainty of $\mathbf{x}_\mathrm{b}$, E{.} stands for the statistical expectation operator and $\mathrm{E}\{\boldsymbol{\varepsilon}_\mathrm{b}\}=0$ means that the mean value of $\boldsymbol{\varepsilon}_\mathrm{b}$ is zero. $\mathbf{B}$ represents the VCM of $\mathbf{x}_\mathrm{b}$ or the background VCM, and finally σ_b^2 the a priori variance factor of $\mathbf{B}$.

In regional gravity field modelling, Eq. (2a) represents independent estimates of Δg ($\mathbf{x}_\mathrm{b}$) together with their associated VCM, shown as $\mathbf{B}$. These values may originate from a global or regional gravity model, or from the outcome of an integral inversion of gravimetric quantities. In this context, each Δg value can be treated as an individual observation, with its uncertainty fully described by $\mathbf{B}$.

Now, assume that Eq. (1a) is discretised and shown in the following Gauss–Markov model:

$$\mathbf{y}=\mathbf{H}\mathbf{x}+\boldsymbol{\varepsilon}_\mathrm{O}\ \text{with}\ \mathrm{E}\{\boldsymbol{\varepsilon}_\mathrm{O}\}=0\ \text{and}\ \mathrm{E}\left\{\boldsymbol{\varepsilon}_\mathrm{O}\boldsymbol{\varepsilon}_\mathrm{O}^\mathrm{T}\right\}=\sigma_\mathrm{O}^2\mathbf{R} \tag{2b}$$

where $\mathbf{y}$ stands for the vector of observations or T_{rr}, $\boldsymbol{\varepsilon}_\mathrm{O}$ the vector of uncertainty of observations, $\mathbf{R}$ the VCM of T_{rr} and σ_O^2 the a priori variance factor of $\mathbf{R}$. $\mathbf{H}$ is the coefficient matrix, so-called design matrix in geodetic or observation operator in data assimilation literature obtained after discretisation of Eq. (1a) and finally, $\mathbf{x}$ is the vector of unknown parameters, containing Δg.

Since Eq. (2b) is obtained after discretising the integral Eq. (1a), the resulting system is typically ill-conditioned. Regularisation is, therefore, required to stabilise it and suppress noise amplification. When a priori information is available—such as background Δg, shown by $\mathbf{x}_\mathrm{b}$, together with their VCM ($\mathbf{B}$), as described in Eq. (2a)—it is desirable to combine such information with the ill-conditioned system in Eq. (2b) while simultaneously applying regularisation. To achieve this, the following objective function is formulated and minimised with respect to $\mathbf{x}$, ensuring a consistent integration of background information, observations and stabilisation through Tikhonov regularisation:

$$\sigma_\mathrm{b}^{-2}(\mathbf{x}_\mathrm{b}-\mathbf{x})^\mathrm{T}\mathbf{B}^{-1}(\mathbf{x}_\mathrm{b}-\mathbf{x}) +\sigma_\mathrm{O}^{-2}(\mathbf{y}-\mathbf{H}\mathbf{x})^\mathrm{T}\mathbf{R}^{-1}(\mathbf{y}-\mathbf{H}\mathbf{x})+\theta^2\mathbf{x}^\mathrm{T}\mathbf{x}\Rightarrow\min \tag{2c}$$

The first term means that the estimate should be close to the background vector $\mathbf{x}_\mathrm{b}$, the second means the observation equivalent $\mathbf{H}\mathbf{x}$, should be close to the real observation $\mathbf{y}$, $()^\mathrm{T}$ is the matrix transpose operator and the third one the norm of $\mathbf{x}$ should be minimised to control its amplification due to ill-conditioning. θ^2 is the positive value regularisation parameter.

In the following, mathematical models suitable for sequential inversion for estimated $\mathbf{x}$ or analysis vector, regularisation bias, VCM, and variance of unit weight are developed. Let us introduce Lemma 1, which is known as Woodbury's matrix identity. It is useful for algebraic manipulations for deriving sequential models.

Lemma 1 (Woodbury matrix identity). *Let* $\mathbf{A}$ *is an* $n\times n$ *and* $\mathbf{P}$ $k\times k$ *and both non-singular matrices.* $\mathbf{U}$ *is an* $n\times k$, *and* $\mathbf{V}$ $k\times n$ *are matrices of compatible dimensions. Woodbury'*

matrix identity is the following relation among these matrices (Woodbury 1950):

$$(\mathbf{A}+\mathbf{UPV})^{-1}=\mathbf{A}^{-1}-\mathbf{A}^{-1}\mathbf{U}\Big(\mathbf{P}^{-1}+\mathbf{VA}^{-1}\mathbf{U}\Big)^{-1}\mathbf{VA}^{-1}.$$

Now, assume that $\mathbf{x}_\mathrm{b}$ and $\mathbf{B}$ are already available from independent sources, implying that they are fully reliable and unbiased. The only system, which is ill-conditioned is Eq. (2b) because of discretising the integral Eq. (1a). In the following proposition, we introduce a sequential model for the joint solution of Eqs. (2a) and (2b), in which corrective terms—referred to as analysis increments—are added to the background state $\mathbf{x}_\mathrm{b}$. These increments update the background state and yield the combined solution, known as the analysis vector $\mathbf{x}_\mathrm{a}$.

Proposition 1. *The sequential joint solution for Eqs. (2a) and (2b) based on the objective function (2c) is:*

$$\mathbf{x}_\mathrm{a}=\mathbf{x}_\mathrm{b}+\mathbf{K}(\mathbf{y}-\mathbf{H}\mathbf{x}_\mathrm{b})-\alpha(\mathbf{I}-\mathbf{KH})\mathbf{C}^{-1}\mathbf{x}_\mathrm{b}$$

where $\mathbf{x}_\mathrm{b}$ and $\mathbf{x}_\mathrm{a}$ are, respectively, known as background and analysis vector in data assimilation literature; and

$$\mathbf{K}=\mathbf{C}^{-1}\mathbf{H}^{T}(\mathbf{R}+\mathbf{H}\mathbf{C}^{-1}\mathbf{H}^{T})^{-1}\quad\textit{and}\quad\mathbf{C}^{-1}=(\mathbf{I}+\alpha\beta^{-1}\mathbf{B})^{-1}\beta^{-1}\mathbf{B}$$

with $\alpha=\sigma_b^{-2}\theta^2$ and $\beta=\sigma_b^{-2}\sigma_O^2$ as tuning parameters.

Proof. *The solution of the objective function (2c) is derived by taking its derivative with respect to $\mathbf{x}$, equating the results to zero, and solving it for $\mathbf{x}$. In other words, it is a solution based on the Tikhonov regularisation (e.g. Tikhonov and Arsenin 1977):*

$$\mathbf{x}_\mathrm{a}=(\sigma_\mathrm{b}^{-2}\mathbf{B}^{-1}+\sigma_\mathrm{O}^{-2}\mathbf{H}^\mathrm{T}\mathbf{R}^{-1}\mathbf{H}+\theta^2\mathbf{I})^{-1}\Big(\sigma_\mathrm{b}^{-2}\mathbf{B}^{-1}\mathbf{x}_\mathrm{b}+\sigma_\mathrm{O}^{-2}\mathbf{H}^\mathrm{T}\mathbf{R}^{-1}\mathbf{y}\Big).\tag{3a}$$

Let us factorise σ_O^{-2}, in this case, Eq. (3a) changes to

$$\mathbf{x}_\mathrm{a}=\mathbf{M}^{-1}\big(\beta\mathbf{B}^{-1}\mathbf{x}_\mathrm{b}+\mathbf{H}^\mathrm{T}\mathbf{R}^{-1}\mathbf{y}\big)\ \text{with}\ \mathbf{M}=\beta\mathbf{B}^{-1}+\mathbf{H}^\mathrm{T}\mathbf{R}^{-1}\mathbf{H}+\alpha\mathbf{I}\tag{3b}$$

with $\beta=\sigma_\mathrm{b}^{-2}\sigma_\mathrm{O}^2$ and $\alpha=\theta^2\sigma_\mathrm{O}^2$ are known as tuning parameters. The term $\mathbf{y}-\mathbf{H}\mathbf{x}_\mathrm{b}$ is referred to as the innovation vector.

In order to obtain a mathematical model, to update $\mathbf{x}_\mathrm{b}$ (the analysis increments), we rewrite Eq. (3a) in the following form

$$\mathbf{x}_\mathrm{a}=\mathbf{M}^{-1}\Big(\beta\mathbf{B}^{-1}\mathbf{x}_\mathrm{b}+\mathbf{H}^\mathrm{T}\mathbf{R}^{-1}\mathbf{y}+\alpha\mathbf{x}_\mathrm{b}-\alpha\mathbf{x}_\mathrm{b}+\mathbf{H}^\mathrm{T}\mathbf{R}^{-1}\mathbf{H}\mathbf{x}_\mathrm{b}-\mathbf{H}^\mathrm{T}\mathbf{R}^{-1}\mathbf{H}\mathbf{x}_\mathrm{b}\Big).\tag{3c}$$

By adding and subtracting $\alpha\mathbf{x}_\mathrm{b}$ and $\mathbf{H}^\mathrm{T}\mathbf{R}^{-1}\mathbf{H}\mathbf{x}_\mathrm{b}$ we try to create $\mathbf{M}$ as a coefficient matrix to $\mathbf{x}_\mathrm{b}$, this will give the possibility of extracting $\mathbf{x}_\mathrm{b}$ as a separate vector:

$$\mathbf{x}_\mathrm{a}=\mathbf{x}_\mathrm{b}+\mathbf{M}^{-1}\mathbf{H}^\mathrm{T}\mathbf{R}^{-1}(\mathbf{y}-\mathbf{H}\mathbf{x}_\mathrm{b})-\alpha\mathbf{M}^{-1}\mathbf{x}_\mathrm{b}.\tag{3d}$$

Equation (3d) can be applied directly, as it is already presented in a sequential form. The second and third terms in this equation together represent the analysis increments, which correspond to the corrections applied to the background state. However, to derive a sequential form that aligns more closely with data assimilation or Kalman filtering methods, we need to consider the following:

$$\mathbf{M}=\mathbf{C}+\mathbf{H}^\mathrm{T}\mathbf{R}^{-1}\mathbf{H}\ \textit{where}\ \mathbf{C}=\beta\mathbf{B}^{-1}+\alpha\mathbf{I}\tag{4a}$$

By applying Lemma 1, and considering $\mathbf{C}=\mathbf{A}$, $\mathbf{P}=\mathbf{R}^{-1}$, $\mathbf{U}=\mathbf{H}^\mathrm{T}$ and $\mathbf{V}=\mathbf{H}$, we can write:

$$\mathbf{M}^{-1}=\mathbf{C}^{-1}-\mathbf{C}^{-1}\mathbf{H}^\mathrm{T}\Big(\mathbf{R}+\mathbf{H}\mathbf{C}^{-1}\mathbf{H}^\mathrm{T}\Big)^{-1}\mathbf{H}\mathbf{C}^{-1}.\tag{4b}$$

In order to avoid inverting $\mathbf{B}$ or risking any conditionality issue, we write.

$$\mathbf{C}^{-1}=\Big(\beta\mathbf{B}^{-1}\Big(\mathbf{I}+\alpha\beta^{-1}\mathbf{B}\Big)\Big)^{-1}=\Big(\mathbf{I}+\alpha\beta^{-1}\mathbf{B}\Big)^{-1}\beta^{-1}\mathbf{B}.\tag{4c}$$

Again, based on Eq. (4c), and considering Lemma 1 we have:

$$\begin{aligned}\mathbf{M}^{-1}\mathbf{H}^\mathrm{T}\mathbf{R}^{-1}&=\Big(\mathbf{C}+\mathbf{H}^\mathrm{T}\mathbf{R}^{-1}\mathbf{H}\Big)^{-1}\mathbf{H}^\mathrm{T}\mathbf{R}^{-1}\\&=\mathbf{C}^{-1}\mathbf{H}^\mathrm{T}\Big(\mathbf{R}+\mathbf{H}\mathbf{C}^{-1}\mathbf{H}^\mathrm{T}\Big)^{-1}=\mathbf{K}\end{aligned}\tag{4d}$$

as the Kalman-type gain matrix. Therefore, Eq. (4b) changes to

$$\mathbf{M}^{-1}=(\mathbf{I}-\mathbf{KH})\mathbf{C}^{-1}.\tag{4e}$$

Based on Eqs. (4b), (4d) and (4e) and inserting them into Eq. (3d), the proposition is proved. Q.E.D.

Based on Eq. (3b) and Eq. (4e), the regularisation bias of the solution of a system of equations solved by the Tikhonov regularisation is (Xu et al. 2006):

$$\mathrm{bias}(\mathbf{x})=-\alpha\mathbf{M}^{-1}\mathbf{x}=-\alpha(\mathbf{I}-\mathbf{KH})\mathbf{C}^{-1}\mathbf{x}\tag{4f}$$

and accordingly the bias-corrected (BC) solution is obtained by subtracting the bias from the solution:

$$\mathbf{x}_\mathrm{BC}=\mathbf{x}_\mathrm{a}+\alpha(\mathbf{I}-\mathbf{KH})\mathbf{C}^{-1}\mathbf{x}.\tag{4g}$$

However, as it is observed for obtaining $\mathbf{x}_{\mathrm{BC}}$ the true value $\mathbf{x}$ is required, but we can always use the analysis vector $\mathbf{x}_{\mathrm{a}}$ as an approximation to $\mathbf{x}$. In this case, we commit another bias in estimating $\mathbf{x}_{\mathrm{BC}}$. One point that should be mentioned is that a successful bias correction depends on how well the system of equations is stabilised and how good the estimated $\mathbf{x}_{\mathrm{a}}$ is, because it contains bias. In some cases, bias correction may destroy $\mathbf{x}_{\mathrm{BC}}$. It is necessary that we always be careful about this step.

Proposition 2. *The BC variance–covariance matrix (VCM) of the estimated analysis vector is:*

$$\mathbf{B}_{\mathrm{bc}} = \mathbf{N}\mathbf{M}^{-1} - \alpha\mathbf{M}^{-1}\left(-2\mathbf{I} + \alpha\mathbf{M}^{-1}\right)\mathbf{N}\mathbf{M}^{-1}$$

where $\mathbf{M}^{-1}$ *is the same as Eq. (4e) and* $\mathbf{N} = \mathbf{I} - \alpha\mathbf{M}^{-1}$.

Proof. *Applying error propagation law to Eq. (3b) leads to:*

$$\mathbf{B}_{\mathrm{a}} = \mathbf{M}^{-1}\left(\beta\mathbf{B}^{-1} + \mathbf{H}^{\mathrm{T}}\mathbf{R}^{-1}\mathbf{H}\right)\mathbf{M}^{-1}. \tag{5a}$$

Note that $\mathbf{M}^{-1}$ *is symmetric and* $\left(\mathbf{M}^{-1}\right)^{\mathrm{T}} = \mathbf{M}^{-1}$ *and it can be computed using Eq. (3b) or Eq. (4b).*

Now, it is straightforward to show that

$$\mathbf{M}^{-1}\left(\beta\mathbf{B}^{-1} + \mathbf{H}^{\mathrm{T}}\mathrm{R}^{-1}\mathbf{H}\right) = \mathbf{I} - \alpha\mathbf{M}^{-1} = \mathbf{N}. \tag{5b}$$

Therefore, Eq. (5a) changes to

$$\mathbf{B}_{\mathrm{a}} = \left(\mathbf{I} - \alpha\mathbf{M}^{-1}\right)\mathbf{M}^{-1} = \mathbf{N}\mathbf{M}^{-1}. \tag{5c}$$

Eshagh et al. (2025) developed the BC VCM for the Tikhonov regularisation solution, accordingly we can write:

$$\mathrm{bias}\{\mathbf{B}_{\mathrm{a}}\} = \alpha\mathbf{M}^{-1}\left(-2\mathbf{I} + \alpha\mathbf{M}^{-1}\right)\mathbf{B}_{\mathrm{a}} \tag{5d}$$

By subtracting Eq. (5d) from Eq. (5c) the proposition is proved. Q.E.D.

The estimated variance of unit weight or a posteriori variance factor is needed to scale or tune the VCM based on residuals. Since estimated residuals also contain regularisation bias, therefore, their bias should be computed and reduced to obtain a more realistic variance. The following proposition presents the BC estimate of such a variance.

Proposition 3. *The BC estimate of variance of unit weight based on model (3a) is:*

$$\sigma^2 = \frac{\left[(\mathbf{x}_{\mathrm{b}} - \mathbf{x}_{\mathrm{BC}})^{\mathrm{T}}\beta\mathbf{B}^{-1}(\mathbf{x}_{\mathrm{b}} - \mathbf{x}_{\mathrm{BC}}) + (\mathbf{y} - \mathbf{H}\mathbf{x}_{\mathrm{BC}})^{\mathrm{T}}\mathbf{R}^{-1}(\mathbf{y} - \mathbf{H}\mathbf{x}_{\mathrm{BC}})\right]}{\left(n_{\mathrm{O}} + \alpha^4\mathrm{trace}(\mathbf{M}^{-4})\right)}$$

where n_{O} *is the number of elements of* $\mathbf{y}$ *vectors and* $\mathbf{x}_{\mathrm{BC}}$ *is the BC estimate, already defined in Eq. (4g).*

Proof. *The BC estimate of the analysis vector (4g) is used for estimating the residual vector and based on Xu et al. (2006) the proposition is proved.* Q.E.D.

The BC variance, Proposition 3, should be multiplied to the BC VCM, Proposition 2, for estimating the VCM of $\mathbf{x}_{\mathrm{a}}$. Note that in the original formula of that variance, presented by Xu et al. (2006), the number of unknowns are subtracted from the total number of observations in the denominator of the variance estimator as well, and since the first system (2a) has equal number of observations to the number of unknowns, therefore only the total number of observations of the second system (2b), n_{O}, appeared in the proposition.

4 Sequential integral inversion through ill-conditioned systems

In the previous section, we assumed that $\mathbf{x}_{\mathrm{b}}$ is available and reliable from earlier computations. However, when $\mathbf{x}_{\mathrm{b}}$ is obtained through regularisation, this assumption becomes problematic, since the sequential inversion then relies on a matrix $\mathbf{B}$ that already contains approximation errors. We now consider a more challenging scenario in which two ill-conditioned systems of equations must be combined sequentially. Specifically, consider the following two Gauss–Markov models, both of which have ill-conditioned coefficient matrices and arise from the discretisation of integral equations. Consider such following models:

$$\mathbf{y}_i = \mathbf{H}_i\mathbf{x} + \boldsymbol{\varepsilon}_i \text{ with } \mathrm{E}\{\boldsymbol{\varepsilon}_i\} = 0 \text{ and } \mathrm{E}\left\{\boldsymbol{\varepsilon}_i\boldsymbol{\varepsilon}_i^{\mathrm{T}}\right\} = \sigma_i^2\mathbf{R}_i \tag{6a}$$

$$\mathbf{y}_{i+1} = \mathbf{H}_{i+1}\mathbf{x} + \boldsymbol{\varepsilon}_{i+1} \text{ with } \mathrm{E}\{\boldsymbol{\varepsilon}_{i+1}\} = 0 \text{ and } \mathrm{E}\left\{\boldsymbol{\varepsilon}_{i+1}\boldsymbol{\varepsilon}_{i+1}^{\mathrm{T}}\right\} = \sigma_{i+1}^2\mathbf{R}_{i+1} \tag{6b}$$

where i means the observation set number, the system of Eqs. (6a) is for the i-th set and (6b) for the next one. The parameters of both systems are definable as in Eq. (2b).

The objective function, which should be minimised to obtain a combined solution for both Eqs. (6a) and (6b) is:

$$\begin{aligned}&\sigma_i^{-2}(\mathbf{y}_i - \mathbf{H}_i\mathbf{x})^{\mathrm{T}}\mathbf{R}_i^{-1}(\mathbf{y}_i - \mathbf{H}_i\mathbf{x})\\ &+ \sigma_{i+1}^{-2}(\mathbf{y}_{i+1} - \mathbf{H}_{i+1}\mathbf{x})^{\mathrm{T}}\mathbf{R}_{i+1}^{-1}(\mathbf{y}_{i+1} - \mathbf{H}_{i+1}\mathbf{x}) + \theta_{i+1}^2\mathbf{x}^{\mathrm{T}}\mathbf{x} \Rightarrow \min\end{aligned} \tag{6c}$$

where θ_{i+1}^2 is the regularisation parameter.

The joint solution of both systems minimises the objective function (6c) is:

$$\mathbf{x}_{i+1} = \mathbf{M}_*^{-1}\left(\sigma_i^{-2}\mathbf{H}_i^{\mathrm{T}}\mathbf{R}_i^{-1}\mathbf{y}_i + \sigma_i^{-2}\mathbf{H}_{i+1}^{\mathrm{T}}\mathbf{R}_{i+1}^{-1}\mathbf{y}_{i+1}\right) \tag{6d}$$

with

$$\mathbf{M}_*^{-1} = \left(\sigma_i^{-2}\mathbf{H}_i^{\mathrm{T}}\mathbf{R}_i^{-1}\mathbf{H}_i + \sigma_{i+1}^{-2}\mathbf{H}_{i+1}^{\mathrm{T}}\mathbf{R}_{i+1}^{-1}\mathbf{H}_{i+1} + \theta_{i+1}^2\mathbf{I}\right)^{-1}. \tag{6e}$$

It will not be difficult to conclude that the one-step solution of N systems of equations will be:

$$\mathbf{x}_N = \left(\sum_{j=1}^{N} \sigma_j^{-2}\mathbf{H}_j^{\mathrm{T}}\mathbf{R}_j^{-1}\mathbf{H}_j + \theta_N^2\mathbf{I}\right)^{-1} \sum_{j=1}^{N} \sigma_j^{-2}\mathbf{H}_j^{\mathrm{T}}\mathbf{R}_j^{-1}\mathbf{y}_j. \tag{6f}$$

As observed, if the observations of all sets are available, the joint solution can be obtained by Eq. (6f). However, if the observations are added to the system step by step, the system should be solved sequentially. The mathematical algorithm for such a process is presented in Proposition 4.

Proposition 4. *The sequential joint regularised solution, based on Eqs. (6a) and (6b), is:*

$$\mathbf{x}_{i+1} = \mathbf{x}_i + \mathbf{K}_{i+1}\left(\mathbf{y}_{i+1} - \mathbf{H}_{i+1}\mathbf{x}_i\right) - \left(\theta_i^2 - \theta_{i+1}^2\right)(\mathbf{I} - \mathbf{K}_{i+1}\mathbf{H}_{i+1})\mathbf{D}^{-1}\mathbf{x}_i$$

where $\mathbf{x}_i$ *and* $\mathbf{x}_{i+1}$*, are, respectively, the regularised solutions of system (6a) and the joint solution of (6a) and (6b). Also,*

$$\mathbf{K}_{i+1} = \mathbf{D}^{-1}\mathbf{H}_{i+1}^{\mathrm{T}}\left(\sigma_{i+1}^2\mathbf{R}_{i+1} + \mathbf{H}_{i+1}\mathbf{D}^{-1}\mathbf{H}_{i+1}^{\mathrm{T}}\right)^{-1} \text{ and}$$
$$\mathbf{D} = \sigma_i^{-2}\mathbf{H}_i^{\mathrm{T}}\mathbf{R}_i^{-1}\mathbf{H}_i + \theta_{i+1}^2\mathbf{I}.$$

Proof. *Since, we cannot simply use Lemma 1, as* $\sigma_i^{-2}\mathbf{H}_i^{\mathrm{T}}\mathbf{R}_i^{-1}\mathbf{H}_i$ *is ill-conditioned, the regularised solution of Eq. (6a) based on the Tikhonov regularisation is used:*

$$\mathbf{x}_i = \left(\sigma_i^{-2}\mathbf{H}_i^{\mathrm{T}}\mathbf{R}_i^{-1}\mathbf{H}_i + \theta_i^2\mathbf{I}\right)^{-1}\sigma_i^{-2}\mathbf{H}_i^{\mathrm{T}}\mathbf{R}_i^{-1}\mathbf{y}_i \tag{7a}$$

with θ_i^2 *as the regularisation parameter of i-th system of equations or Eq. (6a).*

By using Eq. (7a), the joint regularised solution of the systems (6a) and (6b) becomes:

$$\mathbf{x}_{i+1} = \mathbf{M}_*^{-1}\left(\sigma_i^{-2}\mathbf{H}_i^{\mathrm{T}}\mathbf{R}_i^{-1}\mathbf{H}_i\mathbf{x}_i + \theta_i^2\mathbf{x}_i + \sigma_{i+1}^{-2}\mathbf{H}_{i+1}^{\mathrm{T}}\mathbf{R}_{i+1}^{-1}\mathbf{y}_{i+1}\right). \tag{7b}$$

In order to obtain a sequential form for Eq. (7b), let us as add and subtract $\theta_{i+1}^2\mathbf{x}_i$ *and* $\sigma_{i+1}^{-2}\mathbf{H}_{i+1}^{\mathrm{T}}\mathbf{R}_{i+1}^{-1}\mathbf{H}_{i+1}\mathbf{x}_i$ *in the second parenthesis of the equation and simplify the result, in this case, Eq. (7b)is rewritten as:*

$$\mathbf{x}_{i+1} = \mathbf{x}_i + \mathbf{M}_*^{-1}\left(\sigma_{i+1}^{-2}\mathbf{H}_{i+1}^{\mathrm{T}}\mathbf{R}_{i+1}^{-1}\left(\mathbf{y}_{i+1} - \mathbf{H}_{i+1}\mathbf{x}_i\right) + \left(\theta_i^2 - \theta_{i+1}^2\right)\mathbf{x}_i\right). \tag{7c}$$

Now, based on Lemma 1, with $\mathbf{D} = \mathbf{A}$, $\mathbf{P} = \sigma_{i+1}^{-2}\mathbf{R}_{i+1}^{-1}$, $\mathbf{U} = \mathbf{H}_{i+1}^{\mathrm{T}}$ *and* $\mathbf{V} = \mathbf{H}_{i+1}$*, we obtain:*

$$\left(\mathbf{D} + \sigma_{i+1}^{-2}\mathbf{H}_{i+1}^{\mathrm{T}}\mathbf{R}_{i+1}^{-1}\mathbf{H}_{i+1}\right)^{-1}\sigma_{i+1}^{-2}\mathbf{H}_{i+1}^{\mathrm{T}}\mathbf{R}_{i+1}^{-1}$$
$$= \mathbf{D}^{-1}\mathbf{H}_{i+1}^{\mathrm{T}}\left(\sigma_{i+1}^2\mathbf{R}_{i+1} + \mathbf{H}_{i+1}\mathbf{D}^{-1}\mathbf{H}_{i+1}^{\mathrm{T}}\right)^{-1} = \mathbf{K}_{i+1} \tag{7d}$$

where

$$\mathbf{D} = \sigma_i^{-2}\mathbf{H}_i^{\mathrm{T}}\mathbf{R}_i^{-1}\mathbf{H}_i + \theta_{i+1}^2\mathbf{I}. \tag{7e}$$

The proposition is proved based on Eq. (7d), (7e), and (7c). Q.E.D.

In the case where k systems are solved before the last one, the k-th sequence of inversion can be estimated using Proposition 4, but the only difference will be (see Eq. 6e):

$$\mathbf{D} = \sum_{j=1}^{k} \sigma_j^{-2}\mathbf{H}_j^{\mathrm{T}}\mathbf{R}_j^{-1}\mathbf{H}_j + \theta_{k+1}^2\mathbf{I}$$

Proposition 5. *The BC VCM of analysis vector based on sequential integral inversion model is:*

$$\mathbf{B}_{\mathrm{BC}} = \mathbf{N}'\mathbf{M}_*^{-1} - \theta_{k+1}^2\mathbf{M}_*^{-1}\left(-2\mathbf{I} + \theta_{k+1}^2\mathbf{M}_*^{-1}\right)\mathbf{N}'\mathbf{M}_*^{-1}.$$

Proof. *The proof is similar to the proof of* Proposition 2*, by setting,* $\mathbf{D} = \mathbf{C}$, $\mathbf{M}_*^{-1} = (\mathbf{I} - \mathbf{K}_{i+1}\mathbf{H}_{i+1})\mathbf{D}^{-1}$ *and* $\mathbf{N}' = \mathbf{I} - \theta_{k+1}^2\mathbf{M}_*^{-1}$. Q.E.D.

Proposition 6. *The BC estimate of variance of unit weight based on model (6d) is:*

$$\sigma^2 = \left[\left(\mathbf{y}_i - \mathbf{H}_i\mathbf{N}'_*\mathbf{x}_{i+1}\right)^{\mathrm{T}}\sigma_i^{-2}\mathbf{R}_i^{-1}\left(\mathbf{y}_i - \mathbf{H}_i\mathbf{N}'_*\mathbf{x}_{i+1}\right) + \left(\mathbf{y}_{i+1} - \mathbf{H}_{i+1}\mathbf{N}'_*\mathbf{x}_{i+1}\right)^{\mathrm{T}}\sigma_{i+1}^{-2}\mathbf{R}_{i+1}^{-1}\left(\mathbf{y}_{i+1} - \mathbf{H}_{i+1}\mathbf{N}'_*\mathbf{x}_{i+1}\right)\right] \Big/ \left(n_i + n_{i+1} - m + \theta_{i+1}^8\,\mathrm{trace}\left(\mathbf{M}_*^{-4}\right)\right)$$

and n_i*,* n_{i+1}*, and m is the number of elements of* $\mathbf{y}_i$*,* $\mathbf{y}_{i+1}$ *and* $\mathbf{x}_{i+1}$ *vectors, respectively, and* $\mathbf{N}'_* = \mathbf{I} + \theta_{k+1}^2\mathbf{M}_*^{-1}$.

Proof. *The proof is evident based on* Xu et al. (2006).

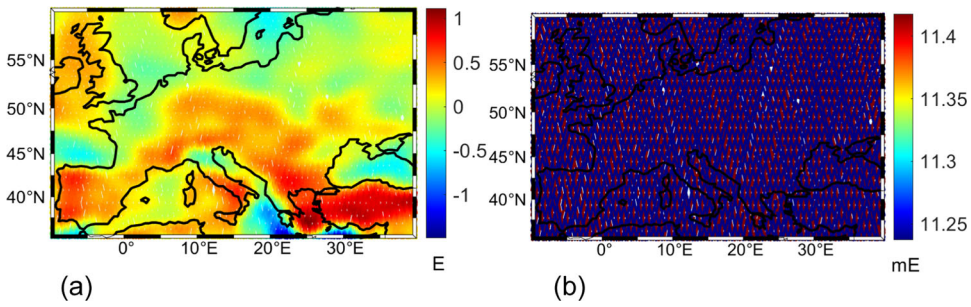

Fig. 1 (**a**) Second-order radial derivatives of disturbing potential (T_{rr}) derived from GOCE data [E], and (**b**) their uncertainties [mE] over study area

5 Numerical experiment

The numerical experiments were conducted over the same central European region used in Eshagh et al. (2025), providing a controlled setting in which differences between batch and sequential inversion can be attributed solely to the estimation methodology. In contrast to earlier studies, the present work uses a substantially larger GOCE T_{rr} data set, sampled at 1-second intervals over a three-month period—approximately ten times the volume typically used in the regional GOCE inversions. To enable sequential processing, the data were divided into multiple subsets, each assimilated in turn by the proposed algorithms. No reduction was applied on the data, allowing the intrinsic behaviour of the sequential inversion framework to be evaluated directly using unreduced GOCE gradients.

5.1 Area and data

A region bounded by latitudes 35° N and 60° N; and longitudes 10° W and 40° E is selected as the study area. The GOCE second-order radial gravity gradients of the product EGG_TRF_2 (EGG-C, 2010) from August to September 2013, are reduced for the normal gravity field, yielding the second-order radial derivative of disturbing potential (T_{rr}) over the area. In total, about 94,540 of the GOCE gradients corresponding with a time resolution of 1 s are used. Figure 1a shows the map of the computed T_{rr}, which ranges from about $-$ 1.5 to 1 Eötvös (E) with large values in the southern part following mountain belts from Turkey and Alp ranges and towards Spain with large values in the south of Italy. Figure 1b is the map of the provided uncertainty of the GOCE gradients and all values are around 11 mE with variations less than 1 mE illustrating a uniform quality of the data.

Our goal is to recover Δg with a spatial resolution of 0.5° $\times$ 0.5° equivalent to a grid size of 100 by 50 or, in other words, 5000 Δg values. Here, the satellite-only combined EGM developed by Zhao et al. (2023) to degree and order 300, from the data of the gravity field and climate experiment (GRACE, Tapley et al. 2004) and GOCE, is considered as a reference. We found that Δg of this EGM commuted to degree 200 is closest to the recovered Δg from the GOCE gradients (e.g. see also Eshagh 2026). The map of Δg computed from this EGM is shown in Fig. 2. This EGM is also used for estimating tuning and regularisation parameters α, β and θ^2 in our computations.

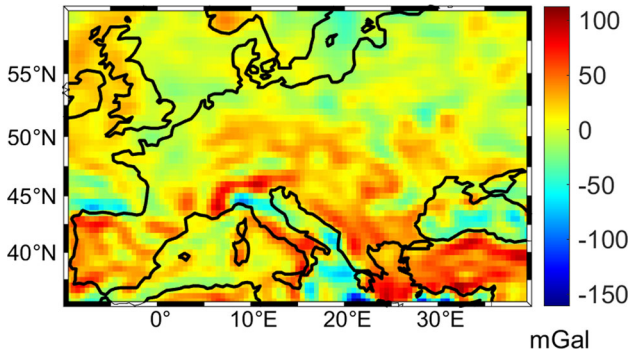

Fig. 2 Map of Δg derived from the combined Earth gravity model (EGM) of Wuhan University determined up to degree and order 200, with a spatial resolution of 0.5° $\times$ 0.5°

5.2 Integral inversion

Considering all 94,540 gradients—or even more—for recovering Δg through the integral formulation would not pose a difficulty when using high-performance computers (HPCs) or supercomputers. However, the objective here is to test and demonstrate the performance of our sequential inversion methods. For this purpose, the complete gradient vector was divided into 10 subsets, which were then inverted sequentially using the proposed approaches. An important criterion in dividing the gradients is that each subset must provide full spatial coverage of the study area. This ensures that, in each inversion sequence, the integral equation can be properly formed to recover all values of Δg on the computational grid, while keeping the spatial truncation error (STE) confined to the margins of the area. To achieve this, a temporal resolution of 10 s was adopted for the gradients, and the subsets were constructed by starting from the first, second, third, and so on up to the tenth element, respectively. In this way, full coverage of the area is guaranteed for every subset. Furthermore, considering the behaviour of the kernel in the

Table 1 Statistics of the differences between EGM Δg and Δg inverted by each set of GOCE gradients [mGal]

	Departure from EGM					Estimated uncertainty				Estimated bias				Estimated RMS			
Set	Max	Mean	Min	STD	RMS	MAx	Mean	Min	STD	Max	Mean	Min	STD	Max	Mean	Min	STD
1	16.9	− 2.8	− 22.0	5.0	5.7	5.9	5.4	4.8	0.3	12.7	0.0	− 17.2	3.2	18.1	6.1	4.9	1.2
2	17.6	− 2.7	− 22.4	5.1	5.8	5.9	5.4	4.9	0.3	10.8	− 0.1	− 17.5	3.2	18.3	6.2	4.9	1.2
3	18.9	− 2.8	− 25.5	5.2	5.9	5.9	5.4	4.9	0.3	11.4	0.0	− 16.4	3.2	17.4	6.1	4.9	1.2
4	18.1	− 2.8	− 24.0	5.3	6.0	5.1	4.7	4.2	0.2	11.7	0.0	− 16.3	3.0	17.0	5.4	4.3	1.1
5	22.1	− 2.8	− 24.7	5.2	5.9	5.9	5.3	4.8	0.3	11.7	0.0	− 16.3	3.1	17.2	6.1	4.8	1.1
6	20.2	− 2.8	− 24.8	4.9	5.7	6.0	5.4	4.9	0.3	11.4	0.0	− 16.6	3.2	17.6	6.2	4.9	1.2
7	14.6	− 2.8	− 24.8	5.0	5.7	5.9	5.4	4.8	0.3	13.2	0.0	− 16.6	3.2	17.6	6.2	4.9	1.2
8	22.6	− 2.8	− 25.4	5.4	6.0	5.4	5.0	4.5	0.2	11.5	0.0	− 16.5	3.0	17.3	5.7	4.5	1.1
9	23.3	− 2.7	− 29.8	5.4	6.1	5.4	5.0	4.5	0.2	11.6	0.0	− 16.6	3.0	17.4	5.7	4.5	1.1
10	19.7	− 2.8	− 26.4	5.2	5.9	5.1	4.7	4.2	0.2	13.8	0.0	− 12.0	3.0	14.7	5.4	4.2	1.1

integral formula (1a), and to reduce the impact of STE, each inversion sequence was performed over the entire study area. However, only the Δg values within a central region—reduced by 3° from each boundary—were retained (see, e.g. Eshagh 2011b; Eshagh et al. 2025). In all experiments, the BC a posteriori variance factors were estimated and subsequently applied to the estimated VCMs, after accounting for and removing the regularisation bias.

5.2.1 Integral inversion of each set

In this section, each set of gradients is inverted to determine their consistency and accuracy in recovering regional Δg from each. Here, the well-known Tikhonov regularisation is applied and its regularisation parameter is estimated in comparison with EGM Δg in the central area. Such a comparison gives us the possibility of assessing the reliability of the satellite-derived gradients before they are integrated into more complex sequential or non-sequential frameworks. Table 1 provides a statistical overview of these residuals, detailing the maximum, minimum, mean, standard deviation (STD), and root mean square error (RMS) for each independent trial, and statistics of estimated uncertainty, bias and RMS.

According to Table 1, the departures of recovered Δg from its EGM counterpart show a consistent pattern across all sets. The means of departures are remarkably stable and close to − 2.8 for all sets, indicating a systematic negative offset relative to the EGM. The STD of the departures lies mostly between 4.9 and 5.4 mGal, and the RMS values are around 5.7–6.1 mGal, suggesting a similar level of variability and overall dispersion across the different data sets despite variations in the extreme values.

The estimated uncertainty is relatively homogeneous across all sets. Maximum uncertainty values are close to 5.9–6.0 mGal, while minimum values range between about 4.2 and 4.9 mGal. The mean uncertainty is consistently around 5.0–5.4 mGal, with small STDs. This indicates that the uncertainty model is stable and does not vary significantly between the different data sets, even when the departure from the EGM exhibits larger extrema. In contrast, the estimated bias shows a wider spread in its extrema. The mean bias is essentially zero for all data sets, and the STD is consistently close to 3.0–3.2 mGal. This suggests that, although local or extreme biases exist, they tend to cancel out, resulting in a negligible overall bias. Finally, the estimated RMS values are quite consistent across all sets. The mean RMS values lie between about 5.4 and 6.2 mGal, which are rather close to the RMS of the departures from the EGM.

5.2.2 Non-sequential integral inversion

This section examines the impact of increasing the data volume on the accuracy of the values of Δg using a non-sequential (or batch) inversion approach. Unlike the previous analysis of individual sets, this method combines multiple GOCE data sets into a single inversion process to evaluate how the inclusion of additional observations refines the resulting Δg. By analysing the cumulative growth of the data from the first two-set combination (1–2) through to the full integration of all ten sets (1–10), we can observe the progressive stabilisation of the Δg recovery and the subsequent reduction in measurement noise.

Table 2 presents statistics of the differences between the recovered Δg from the non-sequential integral inversion, evaluated for progressively cumulative data sets (from 1–2 up to 1–10) and the reference Δg of EGM. The mean value

Table 2 Statistical summary of Δg residuals (in mGal) obtained through non-sequential integral inversion for cumulative data sets (1–2 through 1–10) compared against the EGM reference model

	Departure from EGM					Estimated uncertainty				Estimated bias				Estimated rms				$\times 10^3$
Set	Max	Mean	Min	STD	RMS	Max	Mean	Min	STD	Max	Mean	Min	STD	Max	Mean	Min	STD	θ^2
1–2	17.5	− 2.7	− 19.3	4.6	5.4	4.6	4.2	3.8	0.2	10.7	− 0.1	− 17.6	3.1	18.1	5.0	3.8	1.3	5
1–3	18.5	− 2.7	− 18.3	4.2	5.0	4.2	3.9	3.5	0.2	11.5	− 0.1	− 17.3	2.9	17.7	4.7	3.5	1.3	6
1–4	18.7	− 2.7	− 18.2	4.0	4.9	3.9	3.5	3.2	0.2	11.1	− 0.1	− 17.4	2.9	17.8	4.4	3.2	1.3	7
1–5	19.0	− 2.7	− 17.0	3.9	4.7	3.6	3.3	3.0	0.2	11.5	− 0.1	− 18.5	2.8	18.8	4.1	3.0	1.4	8
1–6	19.6	− 2.7	− 17.4	3.7	4.6	3.5	3.2	2.9	0.2	11.4	− 0.1	− 20.0	2.8	20.3	4.0	2.9	1.4	9
1–7	18.7	− 2.7	− 17.7	3.7	4.6	3.2	3.0	2.7	0.1	11.3	− 0.1	− 20.7	2.8	21.0	3.8	2.7	1.5	10
1–8	18.5	− 2.7	− 17.6	3.6	4.5	3.1	2.8	2.5	0.1	11.2	− 0.1	− 21.0	2.8	21.2	3.7	2.6	1.5	11
1–9	20.3	− 2.7	− 17.6	3.6	4.5	2.9	2.7	2.4	0.1	11.3	− 0.1	− 21.4	2.7	21.6	3.5	2.4	1.5	12
1–10	21.1	− 2.7	− 17.2	3.5	4.4	2.8	2.6	2.3	0.1	11.7	− 0.1	− 21.5	2.7	21.7	3.4	2.4	1.5	13

of departures remains constant at approximately − 2.7 mGal for all cumulative configurations, indicating a persistent and systematic negative offset relative to the EGM Δg. Similar to what we already observed in the inversion of each individual set. Meaning that the systematic bias exists and the increase in data volume does not affect that bias. The STD of the differences decreases steadily from 4.6 to 3.5 mGal, and the RMS reduces from 5.4 to 4.4 mGal.

The estimated uncertainties show a clear and systematic improvement by increasing the data volume. The mean uncertainty also decreases steadily demonstrating that the uncertainty estimates become both lower and more homogeneous with increasing data coverage. This behaviour suggests that the non-sequential inversion effectively reduces uncertainty through cumulative information, which is expected. The estimated regularisation bias statistics indicate that the mean bias is essentially zero for all cumulative data sets. The STD of the bias decreases marginally from about 3.1 to 2.7 mGal, indicating that large biases are localised rather than systematic. Finally, the estimated RMS values show a contrasting trend to the departure RMS. While the maximum RMS increases from approximately 18 to nearly 22 mGal by the data volume, the mean RMS steadily decreases from about 5.0 to 3.4 mGal. The STD of the RMS slightly increases from around 1.3 to 1.5 mGal, reflecting greater spatial variability in extreme RMS values for larger cumulative data sets. These results indicate that the non-sequential integral inversion becomes more accurate on average as additional data are incorporated, even though local extremes may increase due to broader spatial coverage.

The last column lists the estimated regularisation parameters. It shows that, as the size of the system of equations increases, larger regularisation parameters are required to obtain a stable solution. This indicates that the systems become more ill-conditioned as the volume of data increases. However, regularisation is quite successful even when the system becomes slightly more ill-conditioned.

5.2.3 Sequential integral inversion scenarios

In this section, Δg recovery is performed using two distinct sequential inversion scenarios based on the availability and reliability of the VCM and regularisation parameters from preceding steps:

- *Scenario 1.* The VCM from the previous step is utilised with two tuning parameters applied during that stage.
- *Scenario 2.* The VCM is treated as non-definitive, and the observation operators and regularisation parameter from the previous systems are employed instead.

Scenario 1 applies when a priori model of Δg, with its associated VCM, and the specific regularisation parameters from a prior step (e.g. an initial GOCE data set inversion) are all available. In this context, the Tikhonov regularisation is typically used to stabilise the ill-conditioned system, and these parameters are carried forward into the subsequent inversion step following Proposition 1. Scenario 2, based on Proposition 4, is designed for cases where a large dataset is intentionally partitioned into smaller subsets for processing. Since the observation operators derived from the discretisation of the integral formula are internally generated and regularised to ensure stability, they remain fully accessible for the sequential inversion process.

5.2.3.1 Scenario 1 Here, a detailed statistical assessment of the Δg estimation results for Scenario 1 is presented. Our tests showed that in the case of using the regularisation parameter of the previous system as well, like Proposition

Table 3 Statistics of departures of estimated Δg from EGM Δg, along with estimated uncertainty, regularisation bias, and root mean square (RMS) errors for Scenario 1 [mGal]

	Departure from EGM					Estimated Uncertainty				Estimated regularisation bias				Estimated RMS				α	β
Set	Max	Mean	Min	STD	RMS	Max	Mean	Min	STD	Max	Mean	Min	STD	Max	Mean	Min	STD	$\times 10^3$	$\times 10^{11}$
1–2	17.4	− 2.7	− 19.6	4.8	5.5	3.2	2.7	2.4	0.2	19.9	0.0	− 25.6	4.7	25.7	4.8	2.5	2.5	8	1
1–3	18.2	− 2.7	− 20.5	4.4	5.2	3.8	2.4	1.9	0.1	20.1	0.0	− 26.6	4.8	26.7	4.8	2.0	2.9	10	1
1–4	18.9	− 2.8	− 22.0	4.2	5.0	2.7	2.4	2.2	0.1	23.0	0.0	− 30.5	4.8	30.6	4.8	2.2	3.1	11	1
1–5	19.8	− 2.7	− 20.1	4.1	5.0	2.1	1.9	1.7	0.1	24.9	0.0	− 29.8	5.3	29.8	4.6	1.8	3.3	13	1
1–6	20.2	− 2.7	− 19.5	3.9	4.8	2.5	2.2	2.1	0.1	26.5	0.1	− 29.9	5.7	29.9	5.0	2.1	3.5	14	1
1–7	17.9	− 2.8	− 18.7	3.9	4.8	2.0	1.8	1.7	0.1	27.2	0.1	− 30.4	5.8	30.5	4.8	1.7	3.7	16	1
1–8	19.0	− 2.8	− 19.3	3.9	4.8	2.2	2.0	1.9	0.1	28.0	0.1	− 23.3	5.9	32.3	5.0	1.9	3.8	17	1
1–9	22.1	− 2.7	− 19.0	3.9	4.7	2.0	1.8	1.6	0.1	28.6	0.1	− 33.4	6.1	33.5	5.0	1.6	4.0	18	1
1–10	23.2	− 2.7	− 20.8	3.8	4.7	2.1	2.0	1.9	021	30.5	0.1	− 33.6	6.3	33.7	5.2	1.9	4.0	17	1

Tuning parameters α and β are also included for each set

4, a better solution is obtained. To evaluate the performance and reliability of the Δg model.

Table 3 presents similar statistics for the differences between the estimated Δg based on Scenario 1, across different sets and the EGM Δg. The estimated uncertainty, regularisation bias, and RMS of the estimates are also provided in the table. Additionally, the table includes the tuning parameters α and β for each set, which controls the balance between data fitting and smoothing. The table clearly shows that by evolving the datasets, the STD values gradually improve from 4.8 mGal from Set 1–2 to 3.8 mGal sequentially from Set 1 to 10, indicating a reduction in variability and a more consistent model when the number of GOCE data increases. This trend is echoed in the RMS values, which decrease from 5.5 mGal in Set 1–2 to 4.7 mGal and in Set 1–10, suggesting that the Δg model's overall error is improving as the sets progress. Looking at the estimated uncertainty values, we see some fluctuations. For example, the maximum uncertainty starts at 3.2 mGal in Set 1–2 and increases to 3.8 mGal in Set 1–3 fluctuates down to 2.1 in Set 1–10. The minimum uncertainty, however, fluctuates less, ranging from 2.4 to 1.6 mGal. There is a clear trend of increasing regularisation bias, from first its STD is 4.7 mGal and to the last set 6.3 mGal. This increase suggests that the Δg model's regularisation process is becoming more aggressive as the sets progress, potentially introducing larger fluctuations in the estimates. Despite this, the mean bias remains near 0 mGal across all sets, indicating that there is no significant overall bias introduced by regularisation. The estimated RMS has rather stable STD, and relatively increasing trends, and this comes mainly from the estimated regularisation bias. By looking at the mean values of the estimated RMS, which is in fact an internal measure of fit, with the RMS of departures from the EGM, they are rather close to each other and around 5 mGal.

Figure 3a shows the map of differences (or departures) between the recovered Δg and those of the reference EGM. The map reveals a high-frequency, mottled texture, suggesting that the recovered data capture localised variations. Figure 3b presents the histogram of these differences together with the corresponding normal distribution curve. A clear bias is evident, as the centre of the histogram does not coincide with the point under the peak of the normal curve. The positive values of the histogram follow the curve reasonably well, whereas the negative values do not. Examination of the difference map reveals large negative values in the southwestern part of the study area, which are likely remnants of edge effects.

5.2.3.2 Scenario 2 Table 4 provides a detailed statistical analysis of the Δg estimation for Scenario 2. In the first two sets (Set 1–2), the STD and RMS are 4.7 mGal and 5.4 mGal, respectively. The STD values steadily decrease from 4.7 mGal in Set 1–2 to 3.5 mGal in Set 1–10, suggesting an improvement in the model's consistency. The RMS also shows a similar trend, decreasing from 5.4 mGal in Set 1–2 to 4.5 mGal in Set 1–10, reflecting a reduction in overall model error.

The estimated uncertainty has a maximum of 3.2 mGal in Set 1–2, peaks at 3.3 mGal in Set 1–3, and remains fairly stable down to 2.6 mGal across the sets to Set 1–10. The regularisation bias shows a gradual increase, suggesting that regularisation parameters produce bias increasingly. The RMSs follow a similar pattern to the departures, showing a slight reduction as the sets progress. In short, while the

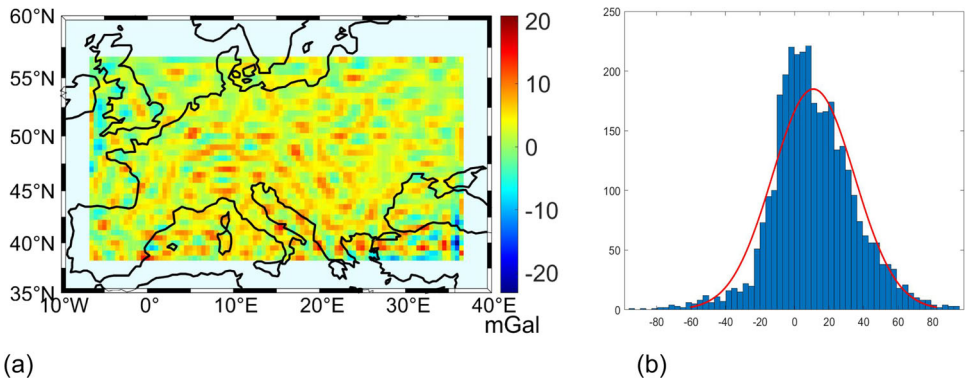

Fig. 3 (**a**) Map of departures between Δg estimated from the sequential integral inversion, Scenario 1, and EGM Δg truncated at degree 200; (**b**) histogram of the departures with the fitted normal distribution curve

Table 4 Statistics of departures of estimated Δg from EGM Δg, along with estimated uncertainty, regularisation bias, and root mean square (RMS) errors for Scenario 2 [mGal]

	Departure from EGM					Estimated Uncertainty				Estimated regularisation bias				Estimated RMS				θ^2
Set	Max	Mean	Min	STD	RMS	Max	Mean	Min	STD	Max	Mean	Min	STD	Max	Mean	Min	STD	$\times 10^3$
1–2	16.5	− 2.7	− 20.2	4.7	5.4	3.2	3.0	2.7	0.1	15.0	− 0.0	− 21.7	3.8	21.9	4.4	2.7	1.9	10
1–3	17.3	− 2.7	− 20.2	4.2	5.0	3.3	3.0	2.7	0.1	13.9	− 0.1	− 21.2	3.5	21.4	4.3	2.7	1.8	10
1–4	18.6	− 2.7	− 20.3	4.0	4.9	3.2	2.9	2.6	0.1	13.8	− 0.1	− 20.5	3.3	20.7	4.1	2.6	1.7	11
1–5	18.7	− 2.7	− 19.1	3.9	4.8	3.0	2.8	2.5	0.1	13.5	− 0.1	− 19.7	3.2	19.9	3.9	2.5	1.7	12
1–6	18.5	− 2.7	− 17.5	3.8	4.7	2.9	2.7	2.4	0.1	13.2	− 0.1	− 20.2	3.1	20.4	3.8	2.4	1.7	13
1–7	17.8	− 2.7	− 17.5	3.7	4.6	2.8	2.6	2.4	0.1	13.3	− 0.1	− 21.0	3.1	21.2	3.7	2.4	1.7	14
1–8	18.6	− 2.7	− 17.3	3.7	4.6	2.7	2.5	2.3	0.1	12.8	− 0.1	− 21.3	3.1	21.5	3.6	2.3	1.7	15
1–9	20.0	− 2.7	− 17.4	3.6	4.5	2.7	2.5	2.3	0.1	12.8	− 0.1	− 22.2	3.0	22.4	3.5	2.3	1.7	15
1–10	20.8	− 2.7	− 17.5	3.5	4.5	2.6	2.4	2.2	0.1	13.3	− 0.1	− 22.3	3.0	22.5	3.5	2.2	1.7	16

maximum departures and bias tend to increase from Set 1–2 to Set 1–10, the STD and RMS values decrease, indicating that the model is becoming more consistent and accurate by increasing the data.

Figure 4a, b is analogous to Fig. 3a, b, respectively, but correspond to Scenario 2. The residual (or departure) values are slightly smaller, and the histogram is more symmetric with a better fit to the normal distribution curve. Nevertheless, a clear bias remains, as the centre of the histogram does not coincide with the point below the peak of the curve, and—similar to Fig. 3b—the histogram exhibits a leftward skew.

5.2.3.3 Comparison of scenarios 1 and 2 In Tables 3 and 4, the maximum departure of the estimated Δg from the EGM values increases progressively from Set 1–2 to Set 1–10 in both scenarios. However, Scenario 1 consistently exhibits larger departures. For example, the maximum difference in Set 1–2 is 17.4 mGal in Scenario 1 compared with 16.5 mGal in Scenario 2. By Set 1–10, these values rise to 23.2 mGal and 20.8 mGal, respectively. The uncertainty estimates display similar temporal behaviour in both cases but remain systematically higher in Scenario 1. In Scenario 1, the maximum uncertainty decreases from 3.8 mGal in Set 1–3 to about 2.1 mGal by Set 1–10. In Scenario 2, it starts at 3.2 mGal and gradually declines to approximately 2.3 mGal to Set 1–10. Mean and minimum uncertainties remain low and stable throughout, with Scenario 2 maintaining slightly smaller values overall. A comparable pattern is observed in the regularisation bias. Although bias increases as additional sets are introduced in both scenarios, its magnitude remains consistently larger in Scenario 1. This indicates a stronger regularisation effect in that configuration. The RMS errors decrease steadily with the inclusion of more sets, reflecting improved model performance. In Scenario 1, the RMS ranges from 4.8 to 5.2 mGal, while in Scenario 2 it decreases from 4.4 to 3.5 mGal. The slightly lower and more stable RMS values in Scenario 2 further confirm its comparatively better accuracy. Generally, both scenarios follow similar trends across the statistical measures; however, Scenario 2 consistently yields lower departures.

The progressive reduction in RMS is expected within a sequential integral inversion framework, where the estimated VCM from one step is propagated to the next. Because

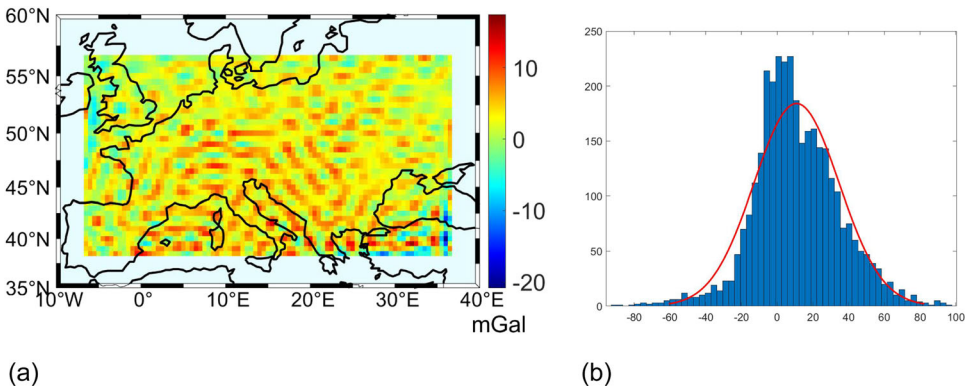

Fig. 4 (**a**) Map of departures between Δg estimated from the sequential integral inversion, Scenario 2, and EGM Δg truncated at degree 200; (**b**) histogram of the departures with the fitted normal distribution curve

each system is ill-conditioned, the estimated variance of unit weight and the VCM inevitably contain regularisation-induced distortions. Although bias-reduction strategies were applied, complete elimination is not feasible, since accurate bias estimation would require knowledge of the true analysis vector, which is unavailable. Consequently, residual distortions persist and are transmitted to subsequent steps. As the VCM plays a central role in determining each new solution, these residual effects accumulate over iterations, providing a plausible explanation for the gradual increase in regularisation bias as the number of sets grows.

Figure 5a shows the map of differences between the Δg model estimated from the two sequential integral inversion approaches, Scenarios 1 and 2. The differences range from approximately -4 to 6 mGal, and their spatial distribution appears largely random. Figure 5b presents the histogram of these differences along with the fitted normal distribution based on their statistical properties. The figure shows a reasonably good agreement between the differences and the normal curve. The histogram is generally symmetric, except for a few values around 6 mGal that fall outside the fitted curve. Notably, unlike the histograms shown in Figs. 4b and 3b, this histogram is not skewed. This indicates that the systematic components in both scenarios are nearly identical; therefore, when one set of the Δg values are subtracted from another, the systematic pattern is effectively eliminated.

5.2.3.4 Scenarios 1 and 2 versus non-sequential integral inversion When comparing the maximum departures from the EGM across the three tables, Scenario 1 (Table 3) consistently exhibits the largest deviations. Both Scenario 2 (Table 4) and the non-sequential integral inversion (Table 2) show smaller and relatively similar magnitudes. As the number of sets increases, departures grow in all approaches, but the increase is more pronounced in Scenario 1, indicating greater variability and deviation from the EGM in this configuration. Minimum and mean values, however, remain comparable across the three methods, suggesting that the main differences lie in the extreme values rather than the central tendency.

A similar pattern emerges in the uncertainty estimates. Scenario 1 systematically produces higher departure than both Scenario 2 and the non-sequential approach. While all methods show broadly stable behaviour across the sets, the consistently larger departure levels in Scenario 1 indicate lower precision relative to the other two strategies even with lower estimated uncertainty. Also, Scenario 1 shows markedly larger bias values throughout all sets, reflecting a stronger influence of the regularisation process. Scenario 2 and the non-sequential inversion exhibit noticeably lower and more comparable bias levels. This suggests that Scenario 1 is more affected by regularisation-induced distortions, potentially introducing greater systematic effects into the solution. Regarding RMS errors, all three methods display gradual improvement as additional sets are incorporated, confirming enhanced model performance over the sequential process. However, Scenario 2 and the non-sequential inversion consistently achieve slightly lower RMS values than Scenario 1. This indicates that, although all approaches benefit from increasing data integration, Scenario 2 and the non-sequential method provide more stable and accurate results overall.

Figure 6 illustrates the performance of sequential integral inversion methods, Scenarios 1 and 2, by mapping the differences in Δg compared to a non-sequential reference approach. Figure 6a, c presents spatial patterns of these differences for the two separate scenarios, localised over Europe and the Mediterranean. The accompanying histograms in Fig. 6b, d show that these differences follow a fitted normal distribution, indicating that the variations are largely statistical in nature. In Scenario 1, the residuals fluctuate within a range of approximately $\pm$ 5 mGal, while Scenario 2 shows a much tighter convergence with differences limited to roughly $\pm$ 2 mGal. These low-magnitude residuals suggest that the sequential inversion technique effectively recovers gravity signals with high accuracy, maintaining strong consistency with standard non-sequential processing methods.

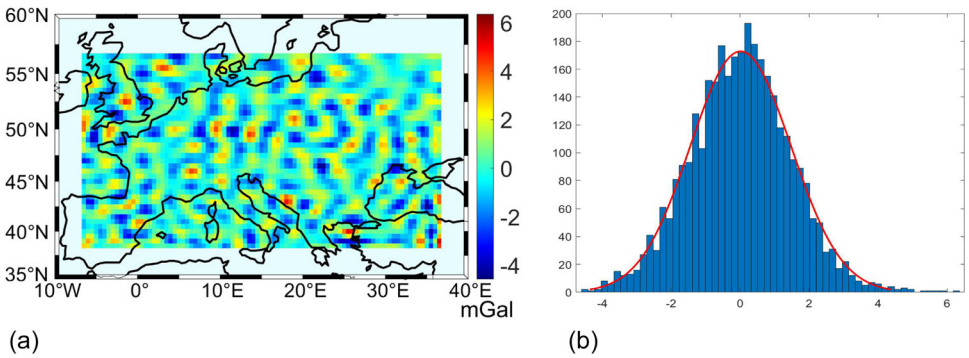

Fig. 5 (**a**) Map of differences between Δg estimated from the sequential integral inversion of Scenario 1 and Scenario 2, (**b**) histogram of the departures with the fitted normal distribution curve

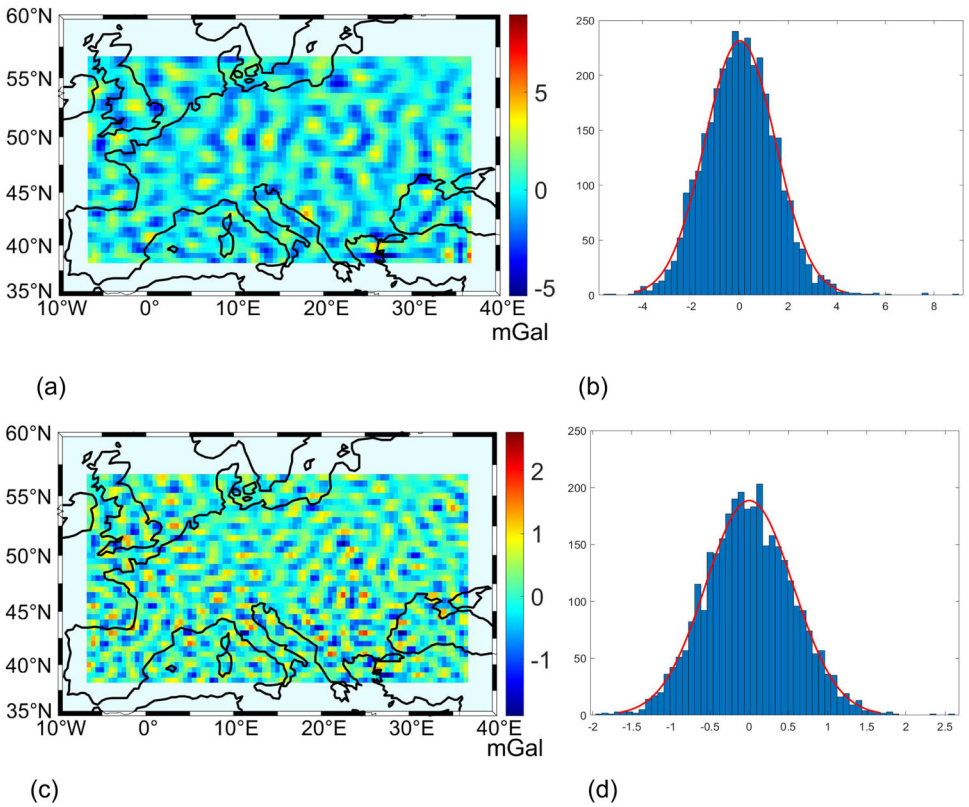

Fig. 6 (**a**) Map of differences between Δg estimated using sequential integral inversion, Scenario 1, and the non-sequential approach; (**b**) histogram and fitted normal distribution of these differences; (**c**) map of differences between Δg estimated using sequential integral inversion, Scenario 2, and the non-sequential approach; and (**d**) histogram and fitted normal distribution of the corresponding differences

6 Discussion

The GOCE data, like any large gravimetric data set, can be partitioned into multiple subsets and processed sequentially. This study has demonstrated two distinct sequential strategies—Scenario 1 and Scenario 2—and compared them with a non-sequential (batch-type) inversion. When each subset is inverted individually, the RMS differences with respect to the EGM-derived Δg remain consistently close, indicating that each block carries comparable information content. This behaviour provides a baseline for interpreting the sequential results. In Scenario 1, each new block is processed using a background Δg and its VCM, which are updated after each step. The increments derived from the observation–model misfit of the next block refine the background estimate. This scenario reflects a genuinely stochastic sequential inversion, where the solution and its uncertainty evolve together. The results show that Scenario 1 converges steadily, but its performance depends strongly on the correct propagation of the tuning parameter and the background VCM. In Scenario 2, the sequential update is applied directly to the accumulated regularised normal equations. Each block contributes a partial normal matrix and right-hand side, which are added to the accumulated system. This approach is algebraically closer to the non-sequential inversion, and the numerical results confirm that Scenario 2 produces Δg estimates that are almost identical to those of the non-sequential inversion. This agreement is expected, because Scenario 2 is theoretically equivalent to solving the full system at once, provided that the tuning parameter is propagated correctly. Proposition 4 plays a crucial role here. It introduces the tuning parameter from the previous step into the update formula, ensuring

that the sequential accumulation remains consistent with the global solution. Without this mechanism, the sequential regularisation may drift or fail.

A key distinction from some earlier studies is that the present work uses real GOCE data with no remove–compute–restore (RCR) reduction and no modification of the integral estimator. These methods place greater emphasis on the selection of the maximum spherical harmonic degree used to remove the long-wavelength component of the gradients. Increasing this degree reduces the magnitude of the residual gradients and lowers the signal-to-noise ratio. For example, Pitoňák et al.(2017) used maximum degrees of 180 and 250, which degraded the reliability of the recovered Δg. Eshagh et al.(2025) used degree 100 to retain more meaningful signal for the RCR method. They also used other direct integral inversion without using the RCR principle but with significantly less amount of data. In the present study, no RCR reduction is applied, but the sequential framework is fully applicable with inversion with RCR and modified integral schemes as the long-wavelength part of the gradients can be removed using an EGM, and the recovered Δg can be restored in the usual way.

Some previous local integral inversion studies that did not use a priori information—such as least-squares collocation or RCR and typically used GOCE gradients sampled at 10-second intervals to limit data volume. The reported standard deviations of about 5 mGal when comparing recovered Δg with an EGM based on the integral inversion (Eshagh 2011a,b,c). In contrast, the present study uses 10 times more data, with a 1-second sampling interval over a three-month period. The proposed sequential algorithms are specifically designed to handle such large data volumes. The results show that the STD can be reduced to approximately 3.5 mGal, and that each additional data subset improves the STD by roughly 0.1 mGal on average.

It is important to distinguish the present methodology from the sequential Tikhonov approach of Eshagh (2011c), which is the closest earlier work. That study estimated a single regularisation parameter from an initial data set and applied it to subsequent systems, removing the regularisation bias at each step. The method was evaluated using simulated data and did not provide a complete sequential formulation. In contrast, the present study develops a fully stochastic sequential inversion framework, with explicit update equations for the solution, the VCM, and the regularisation-induced bias. Scenario 2, in particular, introduces a more sophisticated tuning-parameter strategy that ensures numerical stability and higher precision when applied to real GOCE data. This represents a substantial methodological advance beyond the earlier simulation-based approach.

7 Concluding remarks

This study introduced and evaluated two algorithms for sequential integral inversion, using the recovery of sea-level gravity anomalies (Δg) from GOCE data over Europe as a case study. Although the numerical experiments focussed on this specific application, the proposed framework is general and applicable to the sequential inversion of other gravimetric and geodetic data sets, as well as to the sequential regularisation of large ill-conditioned systems. The first algorithm (Proposition 1) incorporates a priori information on the unknown parameters together with their variance—covariance matrix (VCM). This background information is treated as an independent system in which the parameters are directly observed, conceptually similar to data assimilation algorithms. Because the observational equations arise from discretised integral equations that are inherently ill-conditioned, regularisation is required, and tuning parameters must balance the contributions of the background and observational VCMs. When reliable background information is available from independent sources, this algorithm provides a stable and robust solution. The second algorithm (Proposition 4) does not rely on any external background model or VCM. Instead, it propagates the solution obtained from one data subset to the next, effectively merging multiple ill-conditioned systems in a sequential manner. Although the VCM of the analysis vector can be computed formally, the numerical experiments show that reusing the VCM from a previous step is not advisable, even small biases introduced by regularisation accumulate and amplify during the sequential process, unless there is no other choice. This behaviour was clearly observed in Scenario 1, where discrepancies of up to approximately 5 mGal appeared relative to the non-sequential solution. In contrast, Scenario 2, which sequentially accumulates the regularised normal equations, produced results that agreed with the non-sequential inversion at the 2 mGal level. This agreement reflects the theoretical equivalence between Scenario 2 and the full batch inversion, provided that the tuning parameter is propagated correctly. Proposition 4 plays a central role in ensuring this consistency by linking each sequential step to the previous one. Without this mechanism, the sequential regularisation may fail. Based on these findings, the first algorithm is recommended when trustworthy background information and a reliable VCM are available from independent sources. When no such information exists and the inversion must rely solely on the discretised integral equations, the second algorithm offers a practical and effective alternative. Although sequential inversion requires multiple smaller inversions rather than a single batch solution, it offers a major computational advantage. The peak memory requirement is dramatically reduced. This makes it possible to process large-scale gravimetric data sets on standard workstations, whereas a full batch inversion

may be infeasible due to RAM limitations. The proposed sequential framework is therefore particularly relevant for next-generation gravity missions, where the volume of observations will exceed the capacity of classical batch inversion methods.

Acknowledgements The author is thankful to Docent Dr. Martin Pitonák from the University of West Bohemia, Czech Republic, for preparing the GOCE gradients. Appreciation is also extended to Professor Mirko Reguzzoni, the Associate Editor, and the three anonymous reviewers for their constructive comments and valuable feedback.

Funding Open access funding provided by Swedish Meteorological and Hydrological Institute.

Data availability The datasets generated and/or analysed during the current study are available from the corresponding author on reasonable request.

Open Access This article is licensed under a Creative Commons Attribution 4.0 International License, which permits use, sharing, adaptation, distribution and reproduction in any medium or format, as long as you give appropriate credit to the original author(s) and the source, provide a link to the Creative Commons licence, and indicate if changes were made. The images or other third party material in this article are included in the article's Creative Commons licence, unless indicated otherwise in a credit line to the material. If material is not included in the article's Creative Commons licence and your intended use is not permitted by statutory regulation or exceeds the permitted use, you will need to obtain permission directly from the copyright holder. To view a copy of this licence, visit http://creativecommons.org/licenses/by/4.0/.

References

EGG-C. (2010) GOCE level 2 product data handbook (GO-MA-HPFGS-0110, Issue 4, Rev. 3). European GOCE Gravity Consortium

Eicker A, Schall J, Kusche J (2014) Regional gravity modelling from spaceborne data: case studies with GOCE. Geophys J Int 196(3):1431–1440. https://doi.org/10.1093/gji/ggt485

Eicker A (2008) Gravity field refinement by radial basis functions from in-situ satellite data (Schriftenreihe des Instituts für Geodäsie und Geoinformation, Universität Bonn, No. 10). Universität Bonn

Eshagh M (2011a) Inversion of satellite gradiometry data using statistically modified integral formulas for local gravity field recovery. Adv Space Res 47(1):74–85. https://doi.org/10.1016/j.asr.2010.08.024

Eshagh M (2011b) The effect of spatial truncation error on integral inversion of satellite gravity gradiometry data. Adv Space Res 47:1238–1247. https://doi.org/10.1016/j.asr.2010.11.035

Eshagh M (2011c) Sequential Tikhonov regularisation: an alternative way for integral inversion of satellite gradiometric data. ZfV 136(2):113–121

Eshagh M (2026) Iterative regularisation and uncertainty propagation in solving ill-posed problems: a GOCE-based regional gravity field modelling. Pure Appl Geophys 183:2217–2242. https://doi.org/10.1007/s00024-026-03933-0

Eshagh M, Pitoňák M, Novák P (2025) Uncertainty propagation through integral inversion of satellite gradient data in regional gravity field recovery. J Geod 99:18. https://doi.org/10.1007/s00190-024-01929-z

European Space Agency. (1999) Gravity field and steady-state ocean circulation mission (ESA SP-1233(1)). ESA Publications Division

Janák J, Fukuda Y, Xu P (2009) Application of GOCE data for regional gravity field modelling. Earth Planets Space 61:835–843. https://doi.org/10.1186/BF03353194

Kalnay E, Mote S, Da C (2024) Earth system modeling, data assimilation and predictability: atmosphere, oceans, land and human systems, 2nd ed. Cambridge University Press

Kern M, Haagmans R (2005) Determination of gravity gradients from terrestrial gravity data for calibration and validation of gradiometric GOCE data. In: Gravity, geoid and space missions: GGSM 2004 IAG international symposium Porto, Portugal August 30–September 3, 2004. Springer, pp 95–100. https://doi.org/10.1007/3-540-27604-4_11

Kotsakis C (2007) A covariance-adaptive approach for regularized inversion in linear models. Geophys J Int 171:509–522. https://doi.org/10.1111/j.1365-246X.2007.03534.x

Naeimi M, Bouman J (2017) Contribution of the GOCE gradiometer components to regional gravity solutions. Geophys J Int 209:559–569. https://doi.org/10.1093/gji/ggx040

Pitoňák M, Šprlák M, Novák P, Tenzer R (2017) Regional gravity field modelling from GOCE observables. Adv Space Res 59(1):114–127. https://doi.org/10.1016/j.asr.2016.09.024

Pitoňák M, Novák P, Eshagh M, Tenzer R, Šprlák M (2020) Downward continuation of gravitational field quantities to an irregular surface by spectral weighting. J Geod 94(7):62. https://doi.org/10.1007/s00190-020-01384-6

Pitoňák M, Šprlák M, Ophaug V, Omang OCD, Novák P (2023) Validation of space-wise GOCE gravitational gradient grids using the spectral combination method and GNSS/levelling data. Surv Geophys 44(3):739–782. https://doi.org/10.1007/s10712-022-09762-9

Reed GB (1973) Application of kinematical geodesy for determining the short-wavelength component of the gravity field by satellite gradiometry (Report No. 201). Department of Geodetic Science and Surveying, The Ohio State University

Saadat SA, Safari A, Pitoňák M, Rexer M (2019) Regional gravity field recovery of the void areas using SGG-derived surface residual gravity disturbances based on least squares collocation: a case study in Iran. J Appl Geophys 164:40–52. https://doi.org/10.1016/j.jappgeo.2019.03.002

Schmidt M, Fengler M, Mayer-Gürr T, Eicker A, Kusche J, Sánchez L, Han S-C (2006) Regional gravity modelling in terms of spherical base functions. J Geod 81(1):17–38. https://doi.org/10.1007/s00190-006-0101-5

Tapley BD, Bettadpur S, Watkins M, Reigber C (2004) The gravity recovery and climate experiment: mission overview and early results. Geophys Res Lett 31:1–4. https://doi.org/10.1029/2004GL019920

Tikhonov AN (1963) Solution of incorrectly formulated problems and the regularization method. Sov Math Dokl 4:1035–1038

Tikhonov AN, Arsenin VY (1977) Solutions of ill-posed problems. Wiley

Woodbury MA (1950) Inverting modified matrices (Memorandum Report No. 42). Statistical Research Group, Princeton University

Xu P (1992) Determination of surface gravity anomalies using gradiometric observables. Geophys J Int 110:321–332. https://doi.org/10.1111/j.1365-246X.1992.tb00877.x

Xu P (1998) Truncated SVD methods for discrete linear ill-posed problems. Geophys J Int 135:505–514. https://doi.org/10.1046/j.1365-246X.1998.00652.x

Xu P (2009) Iterative generalized cross-validation for fusing heteroscedastic data of inverse ill-posed problems. Geophys J Int 179:182–200. https://doi.org/10.1111/j.1365-246X.2009.04280.x

Xu P, Shen Y, Fukuda Y, Liu Y (2006) Variance component estimation in linear inverse ill-posed models. J Geod 80:69–81. https://doi.org/10.1007/s00190-006-0032-1

Zhao Y, Li J, Xu X, Su Y (2023) WHU-SWPU-GOGR2022S: a combined gravity model of GOCE and GRACE. GFZ Data Serv. https://doi.org/10.5880/icgem.2023.003

Publisher's Note Springer Nature remains neutral with regard to jurisdictional claims in published maps and institutional affiliations.